Progress In Electromagnetics Research M, Vol. 116, 23–38, 2023

Design and Optimization of Quasi-Constant Coupling Coefficients for Superimposed Dislocation Coil Structures for Dynamic Wireless Charging of Electric Vehicles

Zhongqi Li[1, 3], Xinbo Xiong[2], Liquan Ren[2], Pengsheng Kong[1], Yang Zhang[2, *], and Junjun Li[1, *]

Abstract—In the dynamic wireless charging system of electric vehicles, the misalignment between transmitting and receiving coils will cause drastic changes in the coupling coefficient, which will lead to system instability. A dynamic and static wireless power transfer system superimposed dislocation coil (SDC) structure is proposed in this paper. This structure ensures a constant coupling coefficient between the transmitting and receiving coils of the dynamic and static wireless power transfer system for electric vehicles. Firstly, the variation law of the coupling coefficient of the SDC structure is analyzed. Secondly, a quasi-constant coupling coefficient optimization method is proposed based on the SDC structure to obtain the coil parameters that meet the requirements. Finally, according to the optimization results, an experimental platform for wireless power transfer based on the SDC structure is built. The experimental results show that the maximum fluctuation rate of the inter-coil coupling coefficient is only 3.12% when the misalignment between the transmitting coil and receiving coil is within half of the outer length of the transmitting coil. Thus, the correctness and effectiveness of the proposed structure and method are verified.

1. INTRODUCTION

In recent years, the continuous high oil prices and environmental degradation have led to the rise of a new energy electric vehicle (EV) industry [1–3]. However, the lack of battery capacity can lead to problems such as poor range and slow charging rate of EVs. If electric vehicles are combined with dynamic wireless charging (DWC) technology, the limitations of batteries on electric vehicles can be effectively weakened [4–9]. Coupling coil is a key component in a dynamic wireless charging system. The drastic changes in the system coupling coefficient caused by coil misalignment are the main cause of interference with dynamic wireless charging [10]. The innovation and optimization of the coil structure can fundamentally improve the resistance to misalignment, so it is important to study the new coil structure.

Coil can be divided into single coil structure and multiple coil structure according to the number of coils. In a single coil structure, whether it is a circular or rectangular coil, a misalignment between the transmitting and receiving coils will reduce the positive pair area, resulting in a reduction of the forward magnetic flux. Especially when the misalignment distance reaches half of the side length of the transmitting coil, not only the positive flux will be reduced, but also the negative flux will be generated. This leads to a rapid decrease of the coupling coefficient, which seriously affects the system stability. Therefore, the common single coil structure may not be suitable for dynamic wireless charging.

Received 8 December 2022, Accepted 18 March 2023, Scheduled 29 March 2023

* Corresponding authors: Yang Zhang (hut_zy@163.com), Junjun Li (862739748@qq.com).

[1] College of Railway Transportation, Hunan University of Technology, Zhuzhou 412007, China. [2] College of Electrical and Information Engineering, Hunan University of Technology, Zhuzhou 412007, China. [3] College of Electrical and Information Engineering, Hunan University, Changsha 410082, China.

Multi-coil structure is a structure in which multiple coils are spatially superimposed to achieve the effect of increasing the coupling area between coils by superimposing magnetic fields. Covic of the University of Auckland, New Zealand and other scholars proposed the anti-series Double D (DD) coil structure, which is the more classical of multiple coil structures [11]. The closed magnetic chain formed by the opposite magnetic field is generated by an anti-string coil. Thus, the resistance to misalignment on the Y-axis is enhanced, but it also leads to a magnetic field zero zone. For this reason, Oakland University also proposed to form a Double-D-Quadrature (DDQ) coil by adding a Q-coil in the middle of the DD-coil. Although this overcomes the magnetic field zero-zone problem, it leads to an increase in cost [12]. To reduce the cost, a Bipolar Pad (BPP) coil structure has been proposed by this team. Both BPP type and DDQ type have good anti-misalignment performance in one direction, but the coupling coefficient of BPP type is slightly lower than that of the DDQ type [13]. The Tripolar Pad (TPP) coil has been proposed by [14]. The TPP coil is an improvement based on BPP coil, with greater resistance to misalignment. Taichi coil has been proposed in the literature [15]. This structure is an improvement based on the TPP coil, which has a higher coupling coefficient. The Double Layer Double D-type (DLDD) coil has been proposed in [16]. The DLDD structure further improves the resistance to misalignment, but the fluctuation rate of the coupling coefficient is larger. An asymmetric and reverse series coil structure has been proposed in [17]. This structure is made by winding one coil forward and then reversing the other coil in series. The coil parameters of this structure are optimized to obtain a low coupling coefficient fluctuation rate. In [18], a structure with a rectangular coil reversed in series in the middle of a DD coil connected in the same direction has been proposed. This structure has a strong resistance to misalignment in the Y-axis while improving the coupling coefficient, but the resistance to misalignment in the X-axis is weak. In summary, most of the current coils can only meet the static wireless charging with small misalignment of X-axis and Y-axis or dynamic wireless charging with unidirectional misalignment of Y-axis. Thus, in the case of dynamic wireless charging, the large fluctuation rate of the coupling coefficients at the misalignment of the X-axis and Y-axis remains a problem.

For this reason, a superimposed dislocation coil (SDC) structure is proposed in this paper. It enhances the misalignment resistance in X-axis while satisfying the misalignment resistance in Y-axis. The structure consists of two layers of coils superimposed in a dislocation. Then, a quasi-constant coupling coefficient optimization method is proposed on the basis of the SDC structure. The coil parameters that satisfy the fluctuation rate of the coupling coefficient are obtained by setting constraints. Finally, the correctness of the proposed structure and optimization method is verified by ANSYS Maxwell simulation and experiment. The structure satisfies the requirements of both X-axis and Y-axis misalignment resistance and low coupling coefficient fluctuation rate.

2. CALCULATION OF COUPLING COEFFICIENT

In this section, in order to facilitate the optimization of the coupling coefficient of the proposed SDC structure, a method that can quickly calculate the coupling coefficient of the rectangular coil is used. The expression of the coupling coefficient between two arbitrarily positioned rectangular coils, $\mathrm{Coil_a}$ and $\mathrm{Coil_b}$, is as follows:

$$k = \frac{M_{\mathrm{ab}}}{\sqrt{L_{\mathrm{a}} L_{\mathrm{b}}}} \tag{1}$$

where M_{ab} is the mutual inductance between $\mathrm{Coil_a}$ and $\mathrm{Coil_b}$. L_{a} and L_{b} are the self-inductance of $\mathrm{Coil_a}$ and $\mathrm{Coil_b}$, respectively.

Therefore, it is necessary to calculate the mutual inductance and self-inductance of the coil before calculating the coupling coefficient of the system. Figure 1 shows the schematic diagram of two rectangular coils including $\mathrm{Coil_a}$ and $\mathrm{Coil_b}$. a_1 and a_2 are the length and width of $\mathrm{Coil_a}$. b_1 and b_2 are the length and width of $\mathrm{Coil_b}$. s_1 denotes the vertical distance between O and O_1. s_2 denotes the vertical distance between O and O_2.

According to [17], the expression for the mutual inductance between $\mathrm{Coil_a}$ and $\mathrm{Coil_b}$ can be obtained as follows:

$$\dot{M}_{ab} = \frac{1}{4\pi^2 I} \int_{-\infty}^{\infty} \int_{-\infty}^{\infty} \left(\dot{C}_{\mathrm{x}} + \dot{C}_{\mathrm{z}} \right) \cdot \frac{e^{j(b_{1d}+b_1)\xi} - e^{j(b_{1d}-b_1)\xi}}{j\xi} \cdot \frac{e^{j(b_{2d}+b_2)\eta} - e^{j(b_{2d}-b_2)\eta}}{j\eta} \cdot e^{-qs_2} d\xi d\eta \tag{2}$$

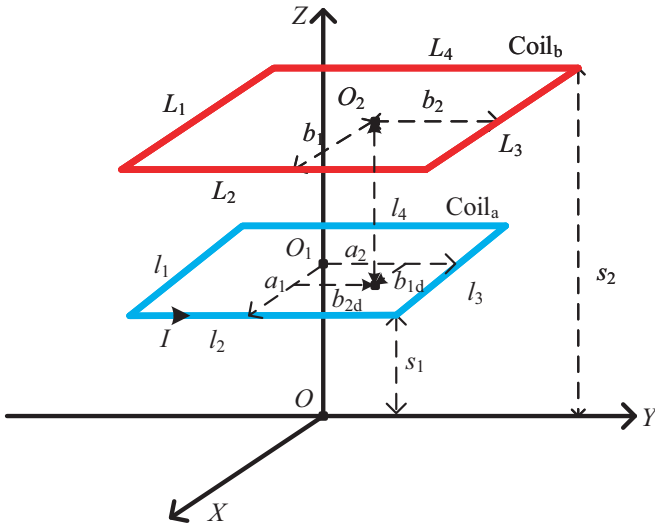

Figure 1. Schematic diagram of two rectangular coils.

where ξ and η are Dual Fourier integral variables; $q = \sqrt{\xi^2 + \eta^2}$; $b_{1\mathrm{d}}$ and $b_{2\mathrm{d}}$ are the misalignments of the X-axis and Y-axis. The expressions for $\dot{C}_{\mathrm{x}}$ and $\dot{C}_{\mathrm{z}}$ are as follows.

$$\dot{C}_{\mathrm{x}} = \frac{-j2\mu_0 I \sin(\xi a_1)\sin(\eta a_2)}{\eta} \cdot e^{s_1 q} \tag{3}$$

$$\dot{C}_{\mathrm{z}} = \frac{-2\mu_0 I q \sin(\xi a_1)\sin(\eta a_2)}{\xi\eta} \cdot e^{s_1 q} \tag{4}$$

The mutual inductance M between multiturn coils can be calculated by (5).

$$M = \left| \sum_{m=1}^{N_a} \sum_{n=1}^{N_b} \dot{M}_{mn} \right| \tag{5}$$

where N_{a} is the number of turns of $\mathrm{Coil_a}$, and N_{b} is the number of turns of $\mathrm{Coil_b}$. m and n turns represent the m-th and n-th turns, respectively. Similarly, the formula for calculating self-inductance can be obtained as follows:

$$\dot{L}_a = \frac{1}{4\pi^2} \int_{-\infty}^{\infty} \int_{-\infty}^{\infty} \int_{-a_1}^{a_1} \int_{-a_2}^{a_2} \frac{-2\mu_0 q \sin(\xi a_1)\sin(\eta a_2)}{\xi\eta} \cdot e^{j(x\xi + y\eta)} dx dy d\xi d\eta \tag{6}$$

$$L = \left| \sum_{m=1}^{N_a} \sum_{n=1}^{N_a} \dot{L}_{mn} \right| \tag{7}$$

According to Eqs. (1), (5), and (7), the coupling coefficients between rectangular coils can be calculated quickly using Matlab. This calculation method is faster than the finite element simulation method. Therefore, a theoretical basis is provided for analysing and optimizing the coupling coefficient of the structure in the next section.

3. SDC STRUCTURAL COUPLING COEFFICIENT CHARACTERISTICS

The SDC structure is capable of achieving a constant coupling coefficient when the X-axis and Y-axis are misaligned. Therefore, this structure enables the electric vehicle to meet the requirements of both dynamic wireless charging and static wireless charging. The SDC structure consists of a transmitting coil and a receiving coil, denoted as $\mathrm{T_x}$ and $\mathrm{R_x}$. $\mathrm{R_x}$ consists of $\mathrm{R_{x1}}$, $\mathrm{R_{x2}}$, $\mathrm{R_{x3}}$ and $\mathrm{R_{x4}}$. As shown in Figure 2(a), the parameter ΔY is the misalignment along the Y-axis, and ΔX is the misalignment along the X-axis.

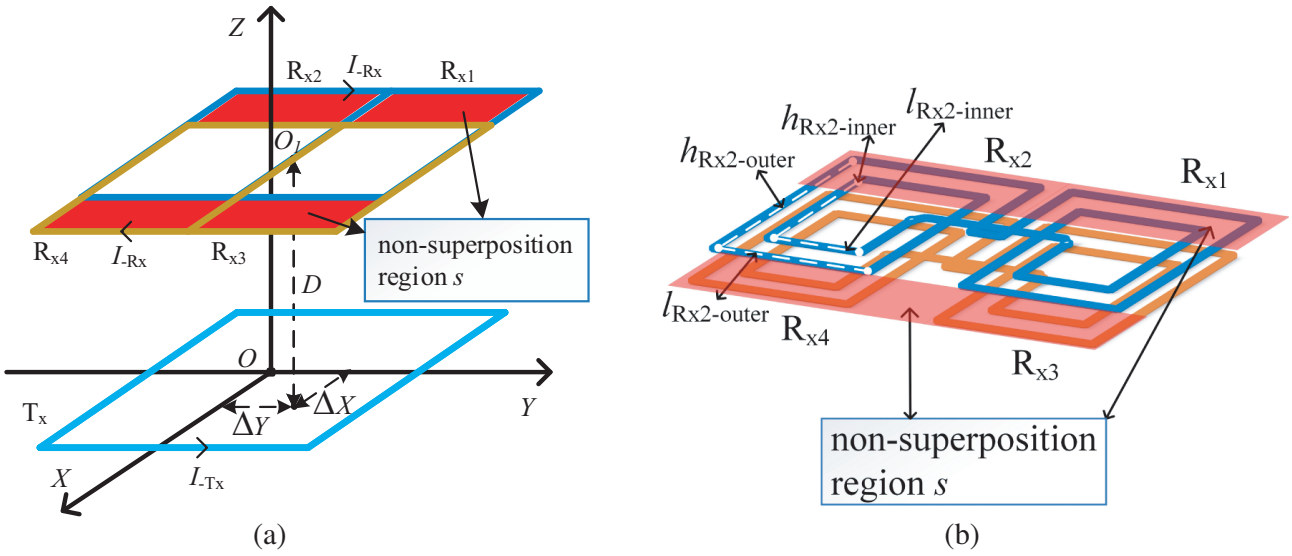

Figure 2. Schematic diagram of superimposed dislocation coil structure. (a) Superimposed dislocation coil structure. (b) Superimposed dislocation coil structure details.

$I_{-\mathrm{Tx}}$ is the current of $\mathrm{T_x}$. $I_{-\mathrm{Rx}}$ is the current of $\mathrm{R_x}$. $\mathrm{R_{x1}}$, $\mathrm{R_{x2}}$, $\mathrm{R_{x3}}$, and $\mathrm{R_{x4}}$ are connected in series in the same direction. That is, the current of $\mathrm{R_{x1}}$ has the same amplitude and phase angle as the currents of $\mathrm{R_{x2}}$, $\mathrm{R_{x3}}$, and $\mathrm{R_{x4}}$. D is the transmission distance between $\mathrm{T_x}$ and $\mathrm{R_x}$. $\mathrm{R_{x1}}$, $\mathrm{R_{x2}}$, and $\mathrm{R_{x3}}$, $\mathrm{R_{x4}}$ are placed superimposed.

There is a non-superposition region between $\mathrm{R_{x1}}$, $\mathrm{R_{x2}}$ and $\mathrm{R_{x3}}$, $\mathrm{R_{x4}}$ with width s.

$$s = \sigma \cdot h_{\mathrm{Rx1-outer}} \tag{8}$$

where σ is the degree of non-superposition between $\mathrm{R_{x1}}$, $\mathrm{R_{x2}}$ and $\mathrm{R_{x3}}$, $\mathrm{R_{x4}}$. $h_{\mathrm{Rx1-outer}}$ is the outer length of $\mathrm{R_{x1}}$.

According to Eq. (5) and Eq. (7), the self-inductance expression of the SDC structure can be obtained as:

$$L = L_{11} + L_{22} + L_{33} + L_{44} + 2M_{13} + 2M_{24} - 2M_{12} - 2M_{14} - 2M_{23} - 2M_{34} \tag{9}$$

where L_{11}, L_{22}, L_{33}, and L_{44} represent the self-inductance of coils $\mathrm{R_{x1}}$, $\mathrm{R_{x2}}$ and $\mathrm{R_{x3}}$, $\mathrm{R_{x4}}$. M_{12}, M_{13}, M_{14}, M_{23}, M_{24}, and M_{34} represent the mutual inductance between the two coils $\mathrm{R_{x1}}$, $\mathrm{R_{x2}}$, $\mathrm{R_{x3}}$, and $\mathrm{R_{x4}}$.

Figure 2(b) is a detailed view of the structure of the receiving coils $\mathrm{R_{x1}}$, $\mathrm{R_{x2}}$, $\mathrm{R_{x3}}$, and $\mathrm{R_{x4}}$. $l_{\mathrm{Rx1-inner}}$, $h_{\mathrm{Rx1-inner}}$, $l_{\mathrm{Rx1-outer}}$, and $h_{\mathrm{Rx1-outer}}$ represent the inner length, inner width, outer length, and outer width of $\mathrm{R_{x1}}$, respectively. Similarly, the parameters of $\mathrm{R_{x2}}$, $\mathrm{R_{x3}}$, $\mathrm{R_{x4}}$, and $\mathrm{T_x}$ are expressed in the same way.

The structure has three features compared to common rectangular coils. Firstly, the size of $\mathrm{T_x}$ is smaller than the size of $\mathrm{R_x}$ to reduce the fluctuation rate of the coupling coefficient. Secondly, $\mathrm{R_{x1}}$, $\mathrm{R_{x2}}$, $\mathrm{R_{x3}}$, and $\mathrm{R_{x4}}$ are all connected in series in the same direction to better couple with the $\mathrm{T_x}$ coil. Third, the four coils $\mathrm{R_{x1}}$, $\mathrm{R_{x2}}$, $\mathrm{R_{x3}}$, and $\mathrm{R_{x4}}$ all have the same structural size, making it easy to optimize the design. When $\mathrm{R_x}$ is misaligned along the positive direction of the Y-axis, the coupling coefficient between $\mathrm{T_x}$ and $\mathrm{R_{x1}}$, $\mathrm{R_{x3}}$ will decrease. The amount of decrease is almost the same as the increase of coupling coefficient between $\mathrm{T_x}$ and $\mathrm{R_{x2}}$, $\mathrm{R_{x4}}$. Therefore, the coupling coefficient between $\mathrm{T_x}$ and $\mathrm{R_x}$ can be kept constant when the misalignment along the Y-axis is within half of the outer length of $\mathrm{T_x}$. Similarly, when $\mathrm{R_x}$ is misaligned along the X-axis, the coupling coefficients between $\mathrm{T_x}$ and $\mathrm{R_{x1}}$, $\mathrm{R_{x2}}$, $\mathrm{R_{x3}}$, and $\mathrm{R_{x4}}$ change in the same way. Therefore, the coupling coefficient between $\mathrm{T_x}$ and $\mathrm{R_x}$ can be kept constant when the misalignment along the X-axis is within 10 cm.

As shown in Figure 3(a), the total coupling coefficient between $\mathrm{T_x}$ and $\mathrm{R_x}$ is not monotonically decreasing when the misalignment distance along the Y-axis increases. Figure 3(a) shows that the

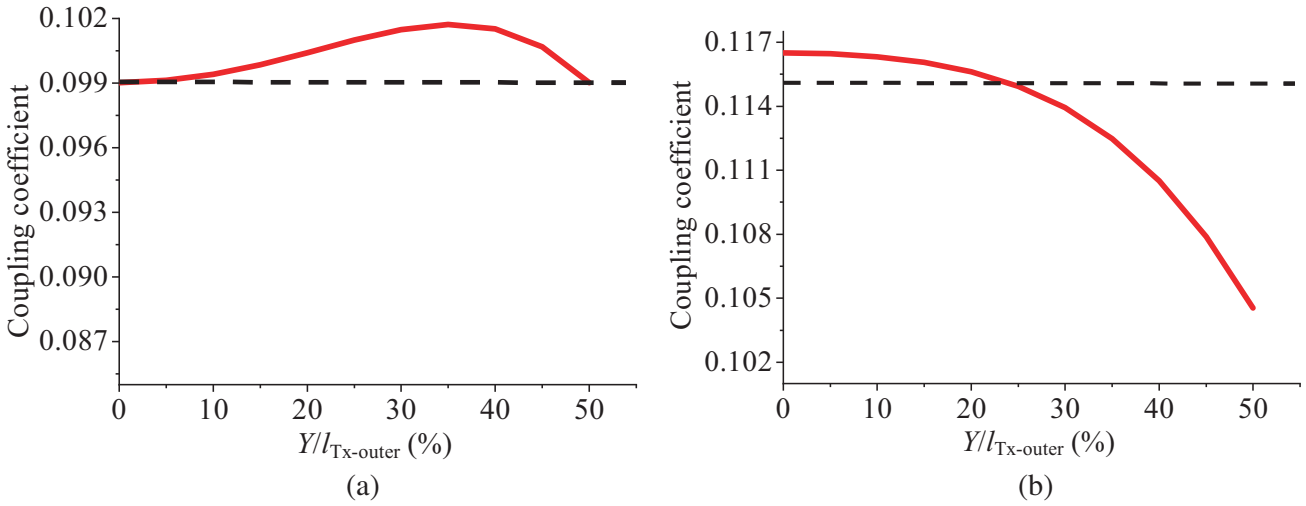

Figure 3. SDC structure and common rectangular coil in Y-axis misalignment coupling coefficient. (a) SDC structure. (b) Common rectangular coil structure.

total coupling coefficient increases when ΔY increases because the increase of the coupling coefficient between T_x and R_{x2}, R_{x4} is greater than the decrease of the coupling coefficient between T_x and R_{x1}, R_{x3}. As shown in Figure 3(b), when both T_x and R_x are common rectangular coils, the coupling coefficient decreases as the degree of misalignment increases. This important finding helps to optimize the coupling coefficient.

4. COUPLING COEFFICIENT OPTIMIZATION METHOD

In this section, a method to obtain quasi-constant coupling coefficients by optimizing the coil parameters is proposed. The optimization results are obtained by using Matlab calculations. The results show that the optimized SDC structure can make the coupling coefficient basically constant.

Equations (1), (5), and (7) show that the coupling coefficient is related to the length, width, and number of turns of the transmitting and receiving coils. The coil parameters are optimized so that the coupling coefficient is quasi-constant within a certain misalignment range. This misalignment range is: Y-axis within half of the outer length of the transmitting coil or X-axis within 10 cm. The optimization flowchart is shown in Figure 4, and the specific steps of the coupling coefficient optimization method are as follows:

(1) Parameters setting and initialization: The transmission distance D between the transmitting coil and receiving coil is set to 15 cm. The number of turns of the receiving coil R_{x1} to R_{x4} is N_{Rx1} to N_{Rx4}. The number of turns of the transmitting coil T_x is N_{Tx}. The diameter of the copper wire is 0.25 cm. ε_{1Y} and ε_{2Y} are the fluctuation rates of the coupling coefficient when the misalignment along the Y-axis is within half of the outer length of the transmitting coil. ε_{1X} and ε_{2X} are the fluctuation rates of the coupling coefficient when the misalignment along the X-axis is within 10 cm.

$$\varepsilon_{1Y} = (k_{Tx-Rx-max-Y} - k_{Tx-Rx-0})/k_{Tx-Rx-0} \tag{10}$$

$$\varepsilon_{2Y} = (k_{Tx-Rx-min-Y} - k_{Tx-Rx-0})/k_{Tx-Rx-0} \tag{11}$$

$$\varepsilon_{1X} = (k_{Tx-Rx-max-X} - k_{Tx-Rx-0})/k_{Tx-Rx-0} \tag{12}$$

$$\varepsilon_{2X} = (k_{Tx-Rx-min-X} - k_{Tx-Rx-0})/k_{Tx-Rx-0} \tag{13}$$

where $k_{Tx-Rx-max-Y}$ and $k_{Tx-Rx-min-Y}$ denote the maximum and minimum coupling coefficients between T_x and R_x when ΔY is within half of the outer length of T_x, respectively. $k_{Tx-Rx-max-X}$ and $k_{Tx-Rx-min-X}$ are the same. $k_{Tx-Rx-0}$ is the coupling coefficient when T_x and R_x are not misaligned.

The standard values of the coupling coefficient fluctuation rates $\varepsilon_{1Y}{}^*$, $\varepsilon_{2Y}{}^*$, $\varepsilon_{1X}{}^*$, and $\varepsilon_{2X}{}^*$ are set to 5%. The standard value of the coupling coefficient $k_{Tx-Rx-0}{}^*$ is set to 0.1.

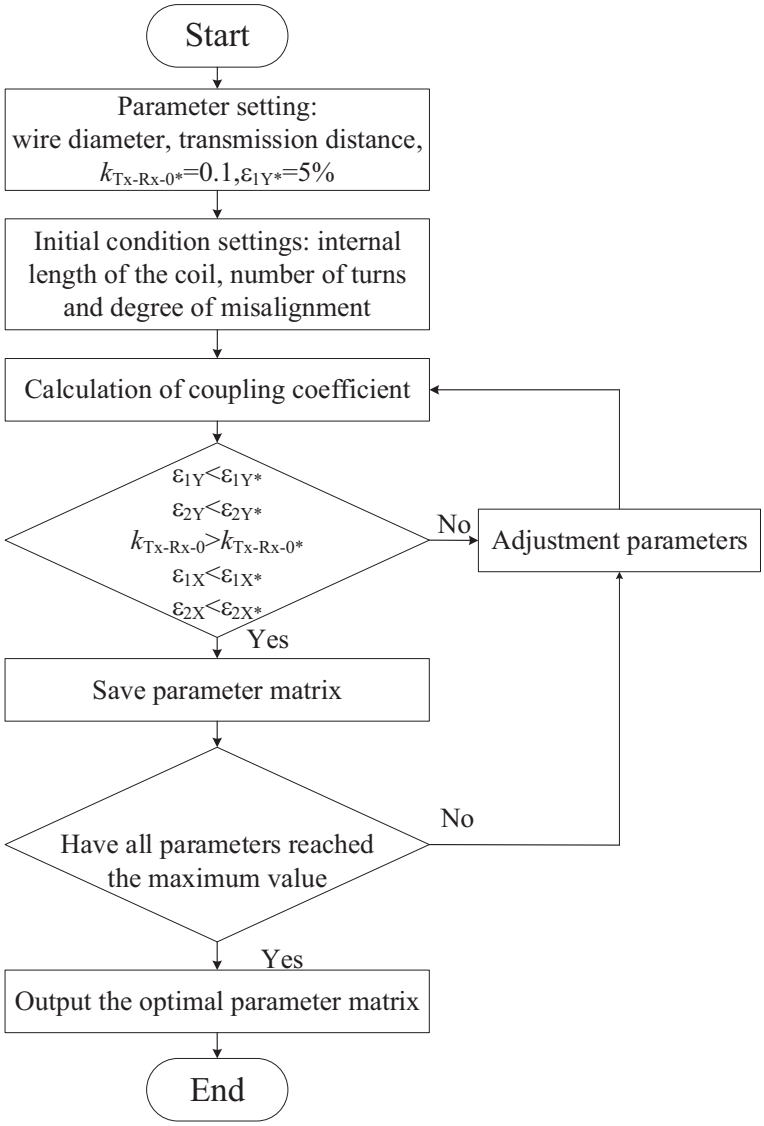

Figure 4. Flow chart of the coupling coefficient optimization method.

(2) Set restrictions: The proposed structures R_{x1}, R_{x2}, R_{x3}, and R_{x4} are of equal dimensions. The inner edge length $l_{Rx1-inner}$ of R_{x1} ranges from 22 cm to 26 cm. The inner edge length $l_{Tx-inner}$ of T_x ranges from 20 cm to 24 cm. The inner edge width $h_{Rx1-inner}$ of R_{x1} ranges from 50 cm to 54 cm. The inner edge width $h_{Tx-inner}$ of T_x ranges from 20 cm to 24 cm. The number of turns N_{Rx1} of R_{x1} ranges from 25 to 29. The number of turns N_{Tx} of T_x ranges from 16 to 20. The degree of non-superposition σ between R_{x1}, R_{x2} and R_{x3}, R_{x4} is 1% to 10%. The number of turns step is 1 turn. The length or width of the step is 1 cm. The non-superposition degree of the steps is 1%.

(3) Coupling coefficient and its fluctuation rate calculation: The coupling coefficients between T_x and R_x can be calculated by Eqs. (1), (5), and (7). ε_{1Y} and ε_{2Y}, ε_{1X} and ε_{2X} can be calculated by Eqs. (10) to (13).

(4) Conditional Judgment: In order to make the SDC structure with quasi-constant coupling coefficients and higher coupling coefficients, the optimization results should satisfy both $\varepsilon_{1Y} < \varepsilon_{1Y}{}^*$, $\varepsilon_{2Y} < \varepsilon_{2Y}{}^*$, $\varepsilon_{1X} < \varepsilon_{1X}{}^*$, $\varepsilon_{2X} < \varepsilon_{2X}{}^*$ and $k_{Tx-Rx-0} > k_{Tx-Rx-0}{}^*$. If the result meets all setting conditions, the result is saved. If all parameters reach their maximum values, the coupling coefficient optimization procedure is terminated. Otherwise, adjust the coil parameters and then return to step 3.

(5) Output optimization results: Record and output all results that meet the requirements.

5. EXPERIMENT VERIFICATION

5.1. Experimental Setup

According to the optimization method proposed in the previous section, the optimization results are obtained using Matlab, and the results are shown in Table 1.

Table 1. Parameters of coils.

Coils	Inner length/cm	Inner width/cm	Outside length/cm	Outside width/cm	Turns
T_x	21	21	35	35	28
R_{x1}	25	54	33	62	16
R_{x2}	25	54	33	62	16
R_{x3}	25	54	33	62	16
R_{x4}	25	54	33	62	16

Figure 5(a) shows the experimental setup including power supply, rectifier-inverter circuit, transmitting coil and SDC receiving coil with its resonant capacitor. The inverter and rectifier circuits all use SiC power devices, model C3M0075120D. The coils used in the experiments are made from 300 strands of AWG 38 Litz wire. The experimental parameters of the SDC structure are shown in Table 2. The physical diagrams of the receiving and transmitting coils of the SDC structure are shown in Figures 5(b) and 5(c). An S-S topology is used for the experimental circuit. The transmission distance D is set to 15 cm, and the resonant frequency is 85 kHz. The IM3536 precision LCR analyzer is used to measure the self and mutual inductance.

Table 2. Measurement parameters of the SDC structure.

Parameter	Physical meaning	Value
L_1/μH	Self-inductance of transmitting coil	371
L_2/μH	Self-inductance of receiving coil	1682
C_1/nF	Compensation capacitance of transmitting coil	9.45
C_2/nF	Compensation capacitance of receiving coil	2.08
Q_1	Quality factor of transmitting coil	680.89
Q_2	Quality factor of receiving coil	377.44
f_0/kHz	Working frequency	85

5.2. Maxwell Simulation and Verification of Coupling Coefficient

The coil simulation model is built in ANSYS Maxwell software using the coil size data in Table 1. The optimization results and the reliability of the SDC structure are verified by simulation, and the simulation model is shown in Figure 6.

In order to verify the correctness of the coupling coefficient calculation method, the following work is performed. Firstly, using Matlab, the calculated value k_c of the coupling coefficients of T_x and R_x can be calculated. Secondly, the simulated value of the coupling coefficient k_s can be obtained from the ANSYS Maxwell simulation model. Finally, the measured parameters of the SDC structure are shown in Table 2. The measured value of the coupling coefficient k_e can be obtained from Eq. (1).

The error between the simulated and calculated values of the coupling coefficient is defined as ε_s, and the error between the measured and calculated values of the coupling coefficient is defined as ε_e.

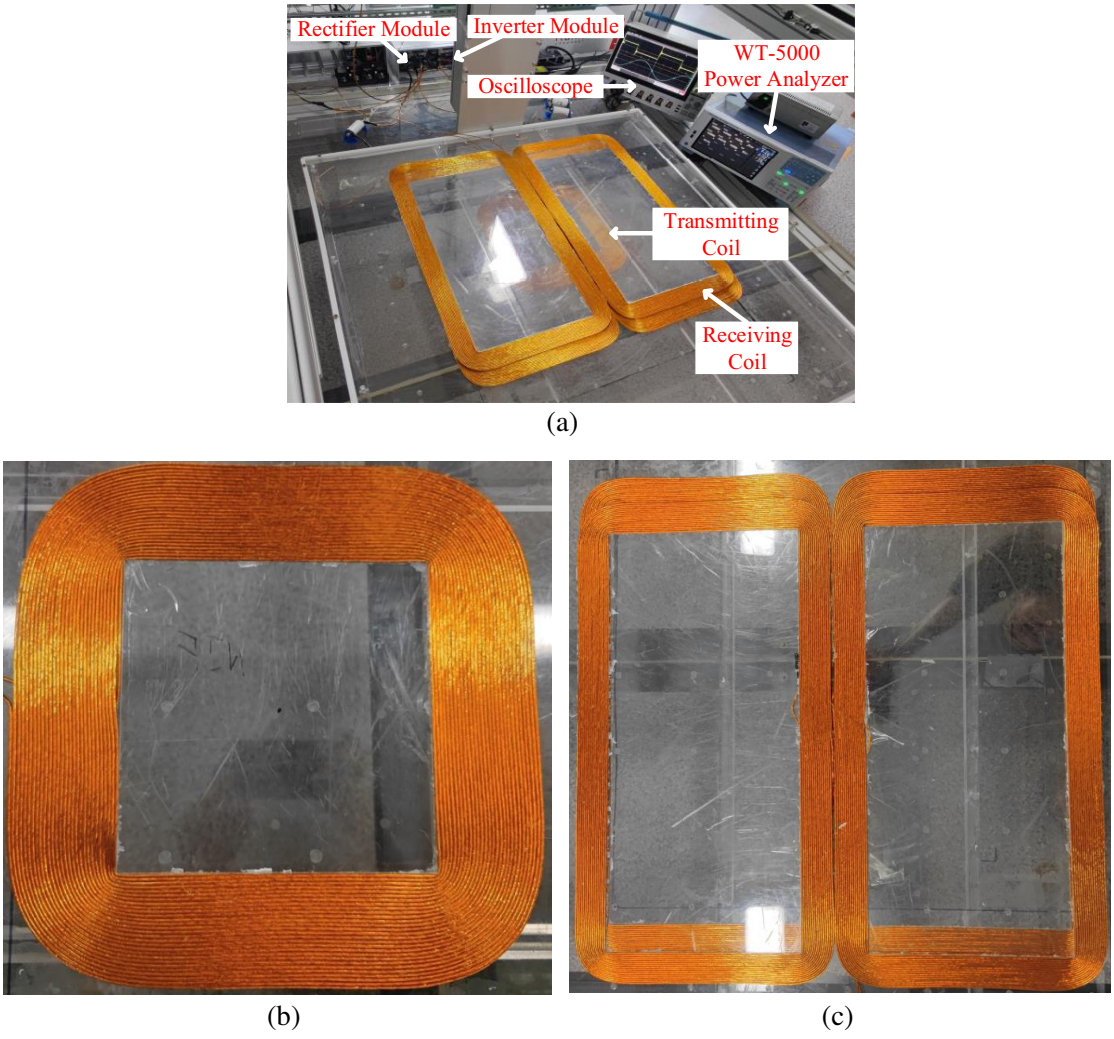

Figure 5. Experimental setup. (a) Overall experimental map. (b) Transmitting coil. (c) Receiving coil.

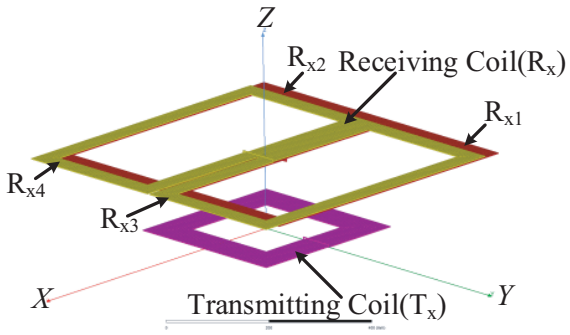

Figure 6. Simulation model.

The two defined equations are as follows.

$$\varepsilon_{\mathrm{s}} = \frac{|k_{\mathrm{c}} - k_{\mathrm{s}}|}{k_{\mathrm{s}}} \times 100 \tag{14}$$

$$\varepsilon_{\mathrm{e}} = \frac{|k_{\mathrm{c}} - k_{\mathrm{e}}|}{k_{\mathrm{e}}} \times 100 \tag{15}$$

Tables 3 and 4 show the calculated value k_c, simulated value k_s, measured value k_e, and error rate of the coupling coefficient when the new coil is misaligned in one direction along the Y-axis and X-axis, respectively. As shown in Table 3, the maximum error rate ε_s between the coupling coefficients k_s and k_c is 3.33%, and the maximum error rate ε_e between the coupling coefficients k_e and k_c is 2.74%. It can be seen from Table 4 that the maximum error rate ε_s between the coupling coefficients k_s and k_c is 3.33%, and the maximum error rate ε_e between the coupling coefficients k_e and k_c is 3.45%. Therefore, it can prove the accuracy of the coupling coefficient calculation method.

Table 3. Calculated, simulated, measured values of coupling coefficient, and error rates with misalignments along the Y-axis in the proposed SDC structure.

Misalignment/cm	k_c	k_s	k_e	$\varepsilon_s/\%$	$\varepsilon_e/\%$
0	0.1086	0.1051	0.1057	3.33	2.74
1.75	0.1087	0.1052	0.1058	3.32	2.74
3.5	0.1088	0.1056	0.1062	3.03	2.45
5.25	0.1091	0.1061	0.1068	2.83	2.15
7	0.1094	0.1062	0.1071	3.01	2.15
8.75	0.1096	0.1074	0.1084	2.05	1.11
10.5	0.1096	0.1072	0.1090	2.72	0.55
12.25	0.1092	0.1073	0.1086	1.77	0.56
14	0.1082	0.1066	0.1079	1.50	0.28
15.75	0.1064	0.1053	0.1066	1.04	0.19
17.5	0.1037	0.1031	0.1047	0.58	0.96

Table 4. Calculated, simulated, measured values of coupling coefficient, and error rates with misalignments along the X-axis in the proposed SDC structure.

Misalignment/cm	k_c	k_s	k_e	$\varepsilon_s/\%$	$\varepsilon_e/\%$
0	0.1086	0.1051	0.1057	3.33	2.74
2	0.1084	0.1050	0.1050	3.24	3.24
4	0.1080	0.1049	0.1044	2.96	3.45
6	0.1071	0.1037	0.1038	3.28	3.18
8	0.1058	0.1030	0.1029	2.72	2.82
10	0.1038	0.1010	0.1024	2.77	1.37

To verify that the coupling coefficient fluctuation rate of the optimized SDC structure can still meet the requirements, Figure 7 is analyzed. From Figure 7(a), it is easy to find that the trend of the coupling coefficient on the Y-axis is saddle-shaped. The center point is lower, and the coupling coefficient increases and then decreases when it is misaligned to both sides. This is different from the trend that the coupling coefficient of common rectangular coils varies inversely with the misalignment distance. When the misalignment distance on the Y-axis is 10.5 cm, the maximum value of the coupling coefficient is 0.1090. When the misalignment distance on the Y-axis is 17.5 cm (half of the outer length of the transmitting coil), the minimum value of the coupling coefficient is 0.1047. When no misalignment occurs, the coupling coefficient is 0.1057. According to Eqs. (10) and (11), the coupling coefficient fluctuation rate can be calculated as $\varepsilon_{1Y} = 3.12\%$ and $\varepsilon_{2Y} = 0.95\%$.

It can be seen in Figure 7(b) that the coupling coefficient of the SDC structure in the X-axis decreases monotonically with increasing misalignment distance. When the misalignment distance in X direction is within 10 cm, the maximum value of coupling coefficient is 0.1057, and the minimum value

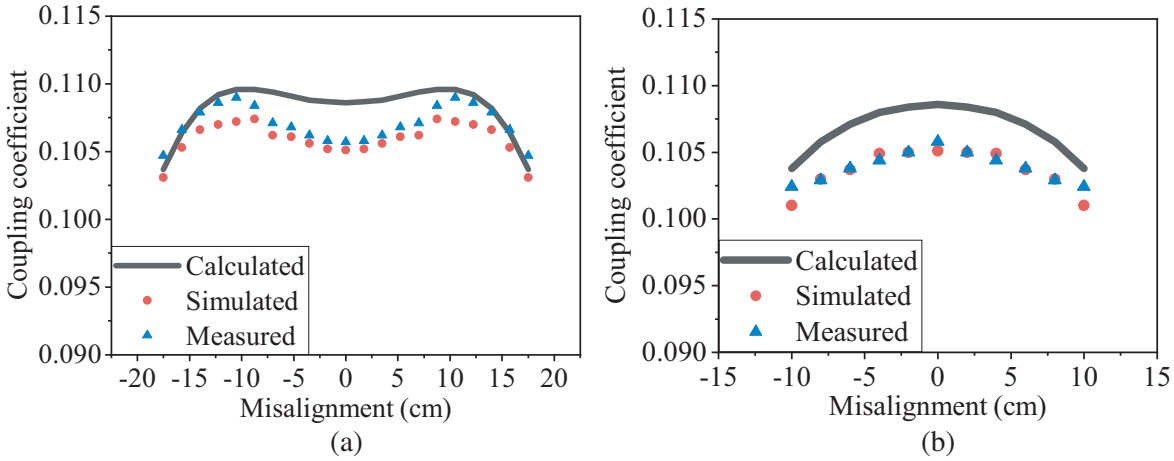

Figure 7. Calculated, simulated and measured values of coupling coefficient of SDC structure. (a) Y-axis. (b) X-axis.

is 0.1024. According to Eqs. (12) and (13), the coupling coefficient fluctuation rate can be calculated as $\varepsilon_{1X} = 0.00\%$ and $\varepsilon_{2X} = 3.12\%$. The results show that the fluctuation rate of the coupling coefficient is less than 5%, regardless of whether the misalignment is along the Y-axis or along the X-axis. Therefore, the SDC structure conforms to the design requirements for dynamic and static wireless charging of electric vehicles.

5.3. Transmission Efficiency and Output Power of SDC Structure

To verify the superiority of the SDC structure as a receiving coil, the transmission efficiency between the transmitting and receiving coils is measured using the WT5000 power analyzer. Figure 8 shows the transmission efficiency and output power of the SDC structure for different misalignment distances along the Y-axis or X-axis. As can be seen in Figure 8(a), the transmission efficiency varies between 97.69% and 94.96%, and the output power varies between 605 W and 557 W when the misalignment distance along the Y-axis is within 17.5 cm. The fluctuation rates of transmission efficiency and output power are 2.79% and 7.93%, respectively. As can be seen in Figure 8(b), the transmission efficiency

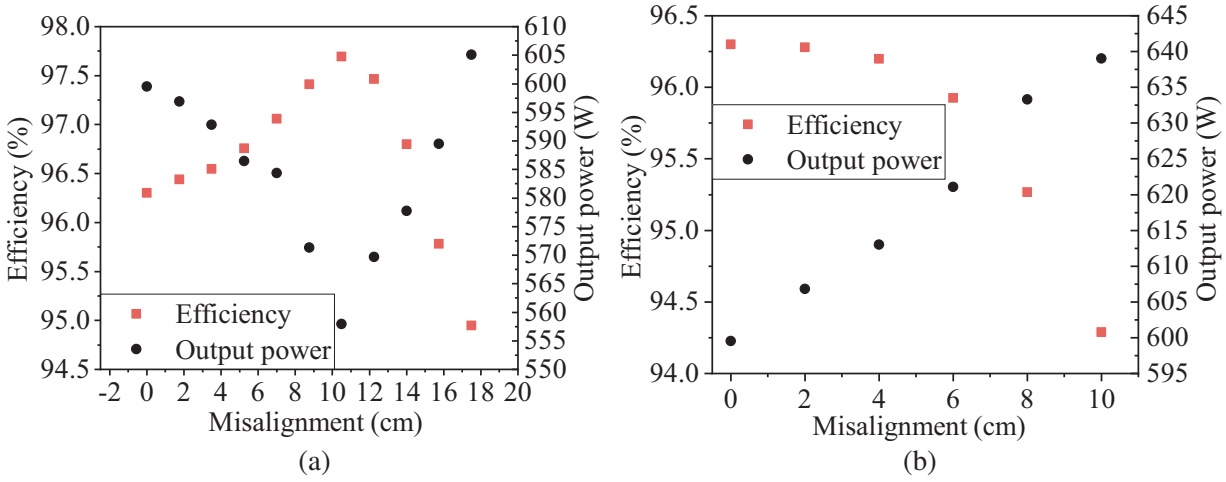

Figure 8. Experimental results of output power and transmission efficiency of SDC structure. (a) Y-axis. (b) X-axis.

varies between 96.30% and 94.29%, and the output power varies between 639 W and 599 W when the misalignment distance along the X-axis is within 10 cm. The fluctuation rates of transmission efficiency and output power are 2.09% and 6.26%, respectively. The results show that the fluctuation rates of transmission efficiency and output power are small when the SDC structure is misaligned. This is because the coupling coefficient is almost constant when the SDC structure is misaligned to different distances along the Y-axis or X-axis.

5.4. Comparison Experiment

To further verify the advantages of this structure, the SDC structure is compared with the common rectangular coil structure. The parameters of the conventional rectangular coil are shown in Table 5, and the common rectangular coil is noted as R_{x5}. Figure 9 shows the coupling coefficient for the common rectangular coil structure. The coupling coefficient decreases from 0.1226 to 0.1062 for a misalignment distance along the Y-axis within 17.5 cm, at which point the coupling coefficient fluctuates by 13.38%. The coupling coefficient fluctuation rate of the common rectangular structure is much larger than that of the SDC structure. A common rectangular coil is used as the receiving coil for simulation verification. Firstly, the resonance of the receiver coil is ensured, and then all other experimental conditions are kept the same as the SDC structure experiment. Since both T_x and R_{x5} are square coil structures, it is sufficient to verify only Y-axis direction. As can be seen from Figure 10, when the misalignment distance is within 17.5 cm, the transmission efficiency changes from 97.73% to 93.81%, and the output power changes from 1473.62 W to 1826.21 W. The fluctuation rate of the output power is 23.93%. The results show that the transmission efficiency and fluctuation rate of the output power of the SDC structure are smaller than those of the common rectangular structure. This is because the coupling coefficient fluctuation rate of the proposed structure is much smaller than that of the common rectangular structure.

The SDC structure is found to have higher copper consumption by comparison. However, the SDC structure has obvious advantages in terms of coupling coefficient fluctuation rate and output

Table 5. Size parameters of common rectangular coils.

Coils	Inner length/cm	Inner width/cm	Outside length/cm	Outside width/cm	Turns	Copper of comparisonr
T_x	21	21	35	35	28	The same
R_{x5}	57	57	66	66	18	44% of SDC

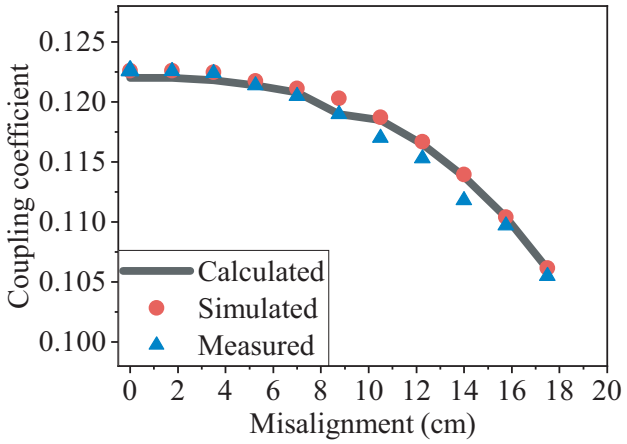

Figure 9. Calculated, simulated and measured values of coupling coefficient of common rectangular structure.

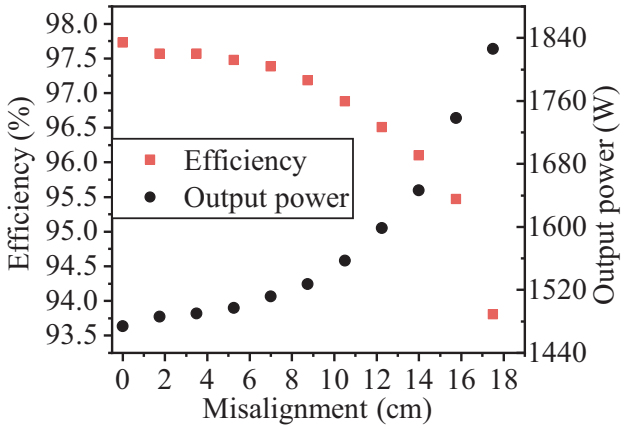

Figure 10. Transmission efficiency and output power of common rectangular structure.

power stability. To demonstrate that the SDC structure is optimized to obtain better performance, the unoptimized coil is compared with the optimized coil. Table 6 shows the parameters of the unoptimized coil. Figure 11 shows the variation of the coupling coefficient of the unoptimized coil compared to the optimized coil. From Figure 11, it is easy to find that there is a significant decrease in the coupling coefficient fluctuation rate after the coil parameters are optimized. Therefore, it is necessary and effective to optimize the coils.

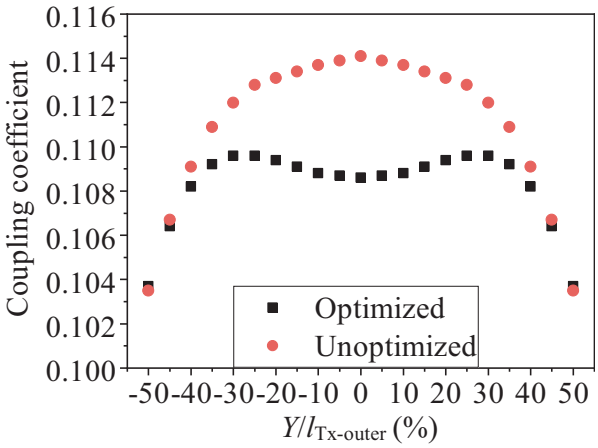

Figure 11. Coupling coefficient of unoptimized coil and optimized coil.

Table 6. Coil size parameters for unoptimized SDC structures.

Coils	Inner length/cm	Inner width/cm	Outside length/cm	Outside width/cm	Turns
T_x	30	30	35	35	10
R_{x1}	23	54	66	66	20

The performance comparison between the proposed SDC structure and the structures proposed in other references is shown in Table 7. Compared with the literature [6, 10, 16], SDC structure has smaller fluctuation rate of coupling coefficient, transmission efficiency, and output power. Without any auxiliary equipment, the efficiency and output power remain almost constant.

Table 7. Performance comparison.

References	Size of Tx (L×W)	Size of Rx (L×W)	Maximum misalignments	Fluctuation of Coupling coefficient	Fluctuation of output power	Fluctuation of efficiency
[6]	30 cm ∗ 20 cm	100 cm ∗ 80 cm	24 cm	/	50.0%	30.0%
[10]	Diameter: 38 cm	Diameter: 60 cm	24 cm	8.4%	14.2%	2.8%
[16]	30 cm ∗ 30 cm	60 cm ∗ 60 cm	20 cm	15.0%	/	/
our work	35 cm ∗ 358 cm	66 cm ∗ 62 cm	17.5 cm	3.12%	7.93%	2.79%

'/' denotes that the value is not given in the references. (Length × width) is abbreviated as $(L \times W)$

5.5. Magnetic Core Research

According to SAE J2954 standard, ferrite materials have been widely used in wireless power transfer systems. Adding a magnetic core can effectively reduce magnetic leakage and improve transmission efficiency [19]. For SDC structure, this section provides a case of adding a magnetic core. The magnetic core structure is shown in Figure 12. The magnetic core parameters are shown in Table 8. The coupling

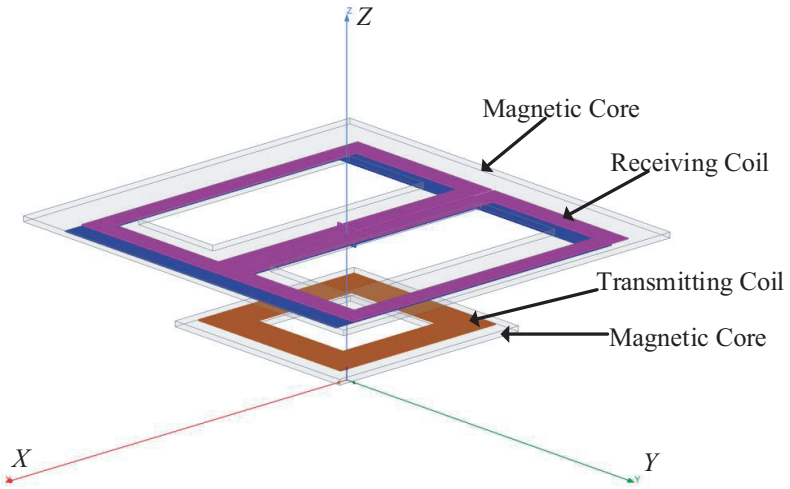

Figure 12. Magnetic core simulation model.

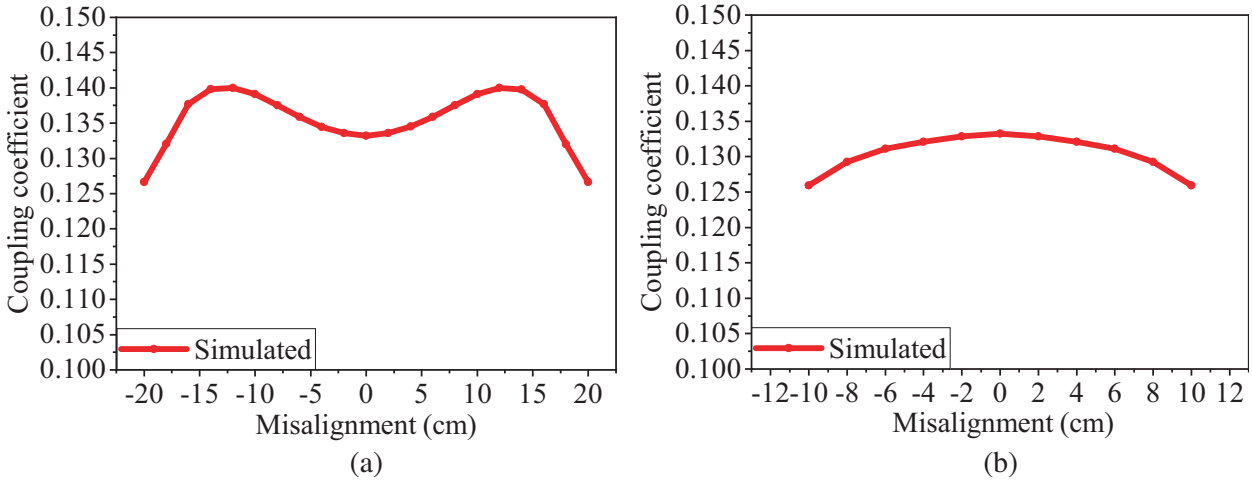

Figure 13. Coupling coefficient of SDC structure with magnetic core. (a) Y-axis. (b) X-axis.

Table 8. Magnetic core parameters.

Parameters of T_x	Value	Parameters of R_x	Value
Outside length	350 mm	Outside length	660 mm
Outside width	350 mm	Outside width	660 mm
Inner length of core	250 mm	Inner length of core	180 mm
Inner width of core	250 mm	Inner width of core	470 mm
Outside length of core	400 mm	Outside length of core	730 mm
Outside width of core	400 mm	Outside width of core	700 mm

coefficient and its change law after adding the core are shown in Figure 13. From Figure 13, it is easy to find that the coupling coefficient is increased significantly after adding the magnetic core, but the coupling coefficient fluctuation rate is still less than 5%. It shows that the SDC structure can still achieve a quasi-constant coupling coefficient with the addition of a magnetic core.

5.6. AC Effect Analysis

The SDC structure is simulated by using ANSYS Maxwell software. As shown in Figure 14, the central cross-section of the SDC structure is taken as the observation surface. Figure 15 shows the loss density distribution of the cross-section of the SDC structure. Since R_{x1}, R_{x2}, R_{x3}, and R_{x4} are all connected in series in the same direction, the currents flow in the same direction. In the cross-section on the left side of the SDC structure, the currents in R_{x2} and R_{x4} flow in the same direction with the same moment. From Figure 15(a), it can be seen that the proximity effect is not obvious, and only the few turns near the outer side of the coil show the proximity effect. It is not difficult to find the same thing on the right side of the SDC structure in Figure 15(b). At the center of the SDC structure, the R_{x2}, R_{x4} are close to R_{x1}, R_{x3}, and meanwhile the currents in R_{x2}, R_{x4} and R_{x1}, R_{x3} flow in reverse. So from Figure 15(c), it can be found that the proximity effect of several turns of coils at the junction of R_{x2}, R_{x4} and R_{x1}, R_{x3} is more obvious. However, the proximity effect of the rest of the coils is not obvious.

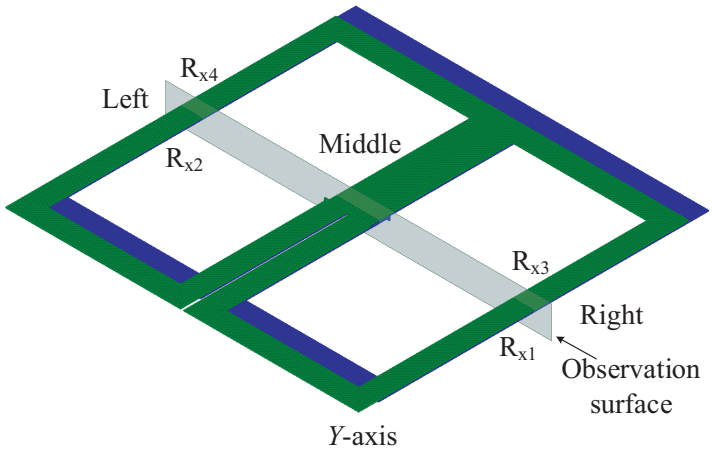

Figure 14. Diagram of observation surface.

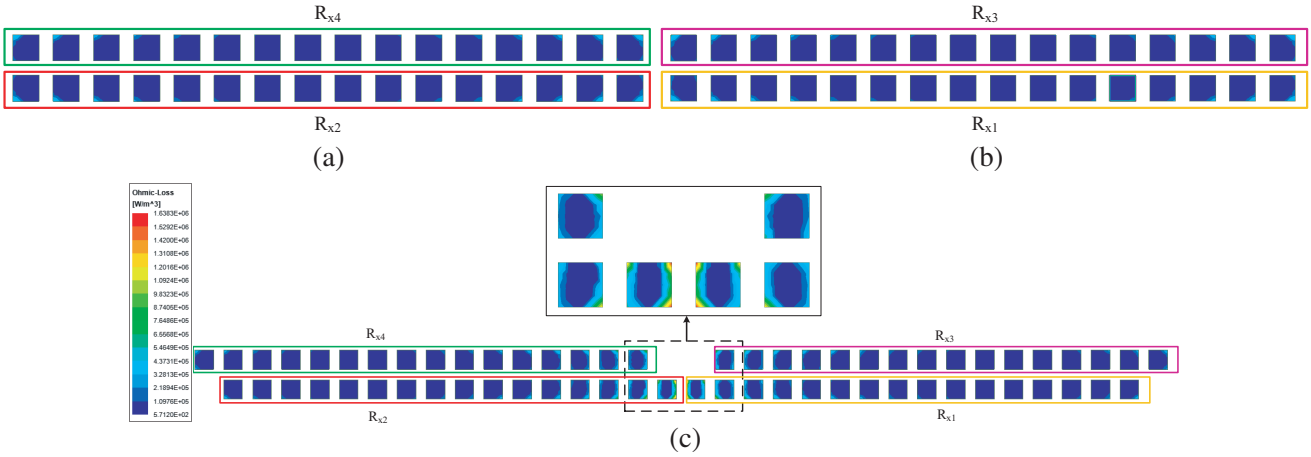

Figure 15. Loss density distribution chart of SDC structure. (a) Left. (b) Right. (c) Middle.

6. CONCLUSION

In this paper, a superimposed dislocation coil structure is proposed. The main feature of an SDC structure is that the decrease in the coupling coefficient between T_x and R_{x1} and R_{x3} at misalignment in the Y-axis is almost the same as the increase in the coupling coefficient between T_x and R_{x2} and R_{x4}. The characteristics on the X-axis of the SDC structure are similar to those on the Y-axis. These features give the SDC structure good misalignment resistance in both the Y-axis and X-axis. In addition, a quasi-constant coupling coefficient optimization method for rectangular coil parameters is proposed.

Maxwell simulations and experiments are performed on the results obtained using the coupling coefficient optimization method. The feasibility and superiority of the coupling coefficient calculation and coupling coefficient optimization scheme are verified. The experimental results show that the coupling coefficient fluctuation rates are both 3.12% when the misalignment of the receiving coil along the Y-axis and X-axis is 17.5 cm and 10 cm, respectively. Also, without the remaining auxiliary devices, the maximum output power fluctuation rate and maximum efficiency fluctuation rate are 7.93% and 2.79%, respectively. The output power and transmission efficiency remain almost constant. Therefore, it can be demonstrated that the SDC structure can be used for dynamic wireless charging and static wireless charging of electric vehicles. The next step is to improve the proposed structure so that it can have a higher coupling coefficient and stronger resistance to misalignment.

ACKNOWLEDGMENT

This work was supported in part by the National Nature Science Foundation of China under Grant 11901188, in part by the Natural Science Foundation of Hunan Province under Grants 2022JJ30226 and 2019JJ60066, in part by the Outstanding Youth Project of Hunan Education Department under Grants 20B186.

REFERENCES

1. Wei, G. and J. Feng, "An efficient power and data synchronous transfer method for wireless power transfer system using double-D coupling coil," *IEEE Transactions on Industrial Electronics*, Vol. 68, No. 11, 10643–10653, Nov. 2021.
2. Mohammed, S. A. Q. and J. W. Jung, "A comprehensive state-of-the-art review of wired/wireless charging technologies for battery electric vehicles: Classification/common topologies/future research issues," *IEEE Access*, Vol. 9, 19572–19585, Jan. 2021.
3. ElGhanam, E. and H. Sharf, "On the coordination of charging demand of electric vehicles in a network of dynamic wireless charging systems," *IEEE Access*, Vol. 10, 62879–62892, Jun. 2022.
4. Farajizadeh, F. and D. M. Vilathgamuwa, "Expandable N-legged converter to drive closely spaced multitransmitter wireless power transfer systems for dynamic charging," *IEEE Transactions on Power Electronics*, Vol. 35, No. 14, 3794–3806, Apr. 2020.
5. Mahesh, A. and B. Chokkalingam, "Inductive wireless power transfer charging for electric vehicles — A review," *IEEE Access*, Vol. 9, 137667–137713, Sep. 2021.
6. Choi, S. and S. Jeong, "Ultraslim S-type power supply rails for roadway-powered electric vehicles," *IEEE Transactions on Power Electronics*, Vol. 30, No. 11, 6456–6468, Nov. 2015.
7. Ahmad, A., M. Alam, and R. Chabaan, "A comprehensive review of wireless charging technologies for electric vehicles," *IEEE transactions on transportation electrification*, Vol. 4, No. 1, 38–63, Mar. 2017.
8. Jeong, S. and Y.J. Jang, "Charging automation for electric vehicles: Is a smaller battery good for the wireless charging electric vehicles?," *IEEE Transactions on Automation Science and Engineering*, Vol. 16, No. 1, 486–497, Jan. 2019.
9. Zhang, X. and Z. Yuan, "Coil design and efficiency analysis for dynamic wireless charging system for electric vehicles," *IEEE Transactions on Magnetics*, Vol. 52, No. 7, 1–4, Jul. 2016.

10. Li, Z. and J. Yi, "Modeling and design of a transmission coil and four cascaded receiving coils wireless charging structure with lateral misalignments," *IEEE Access*, Vol. 8, 75976–75985, Apr. 2020.
11. Budhia, M., G. Covic, J. T. Boys, and C.-Y. Huang, "Development and evaluation of single sided flux couplers for contactless electric vehicle charging," *2011 IEEE Energy Conversion Congress and Exposition*, 614–621, Oct. 2011.
12. Budhia, M. and J. T. Boys, "Development of a single-sided flux magnetic coupler for electric vehicle IPT charging systems," *IEEE Transactions on Industrial Electronics*, Vol. 60, No. 1, 318–328, Jan. 2013.
13. Zaheer, A. and G. A. Covic, 'A bipolar pad in a 10-kHz 300-W distributed IPT system for AGV applications," *IEEE Transactions on Industrial Electronics*, Vol. 61, No. 7, 3288–3301, Jul. 2013.
14. Kim, S. and G. A. Covic, "Tripolar pad for inductive power transfer systems for EV charging," *IEEE Transactions on Power Electronics*, Vol. 32, No. 7, 5045–5057, Jul. 2017.
15. Li, Y. and J. Zhao, "A novel coil with high misalignment tolerance for wireless power transfer," *IEEE Transactions on Magnetics*, Vol. 55, No. 6, 1–4, Jun. 2019.
16. Wang, Z. and C. Hu, "Design of magnetic coupler for inductive power transfer system based on output power and efficiency," *Transactions of China Electrotechnical Society*, Vol. 30, No. 19, 26–31, 2015.
17. Li, Z. and J. Li, "Design and optimization of asymmetric and reverse series coil structure for obtaining quasi-constant mutual inductance in dynamic wireless charging system for electric vehicles," *IEEE Transactions on Vehicular Technology*, Vol. 71, No. 3, 2560–2572, 2021.
18. Li, Z. and S. Li, 'Mutual inductance calculation and optimization of multi-receiver positive and negative series coil structure in dynamic wireless power transfer systems," *Transactions of China Electrotechnical Society*, Vol. 36, No. 24, 5153–5164, 2021.
19. Otomo, Y. and H. Igarashi, "A 3-D topology optimization of magnetic cores for wireless power transfer device," *IEEE Transactions on Magnetics*, Vol. 55, No. 6, 1–5, Jun. 2019.